

Changes in stress state and seismicity pattern responsible for the 2019 Ridgecrest, California, earthquakes

Kazuyoshi Nanjo¹

¹University of Shizuoka

November 24, 2022

Abstract

Monitoring stress state in the Earth's crust plays a crucial role in our understanding of an earthquake's mechanism, especially how earthquake ruptures nucleate, as well as in calculating the distribution of hazards. Crustal deformation due to the 2019 Ridgecrest earthquakes, which occurred near the town of Ridgecrest, California, that culminated in a preceding earthquake of magnitude (M) 6.4 and a subsequent M7.1 event, caused stress perturbation in nearby regions. However, implications of future seismic activity are still unclear. Here we analyze the occurrence of small earthquakes compared to larger ones—the b-values, showing how the nucleation area for both the M6.4 and M7.1 earthquakes had low b-values before these events occurred, and mid-to-high b-values thereafter. The slip distribution of the M7.1 event is also well correlated with the b-value map. Additionally, the time and local-dependent variations in b-values of the Ridgecrest earthquakes are linked with estimates of changes to Coulomb stress. The main conclusion is that the b-value mapping provide insight into the stress state in the fault zone, which is likely closely related to the nucleation and evolution of earthquakes in the sequence. The combined approach of stress-change and b-value analyses to the post-M7.1-quake sequence shows an area that is currently being stressed near the Garlock fault that hosted past large earthquakes. The b-values are not as low as those immediately before the M6.4 and M7.1 events, but contribute the most recent values in a decreasing trend of the b-value. Together with geodetic and seismological observations, monitoring the spatial and temporal distribution of b-value would contribute to seismic hazards in the Eastern California Shear Zone.

Changes in stress state and seismicity pattern responsible for the 2019 Ridgecrest, California, earthquakes

K. Z. Nanjo

University of Shizuoka, Japan (nanjo@u-shizuoka-ken.ac.jp)

PRESENTED AT:



OBJECTIVE

- Promote better understanding of earthquake's mechanism, especially how earthquake ruptures nucleate.
- Analyze seismicity and crustal deformation due to the 2019 Ridgecrest earthquakes, which occurred near the town of Ridgecrest, California, that culminated in a preceding earthquake of magnitude (M) 6.4 and a subsequent $M7.1$ event.
- Apply the occurrence of small earthquakes compared to larger ones, the b -values, to the Ridgecrest case, showing that the b -value mapping provides insight into the stress state in the fault zone, which is likely closely related to the nucleation and evolution of earthquakes in the sequence.
- The combined approach of stress-change and b -value analyses to the post- $M7.1$ -quake sequence shows an area that is currently being stressed near the Garlock fault that hosted past large earthquakes.

Reference

Nanjo, K.Z. Were changes in stress state responsible for the 2019 Ridgecrest, California, earthquakes?. Nat Commun 11, 3082 (2020). <https://doi.org/10.1038/s41467-020-16867-5>

RIDGECREST EARTHQUAKE SEQUENCE AND B-VALUES.

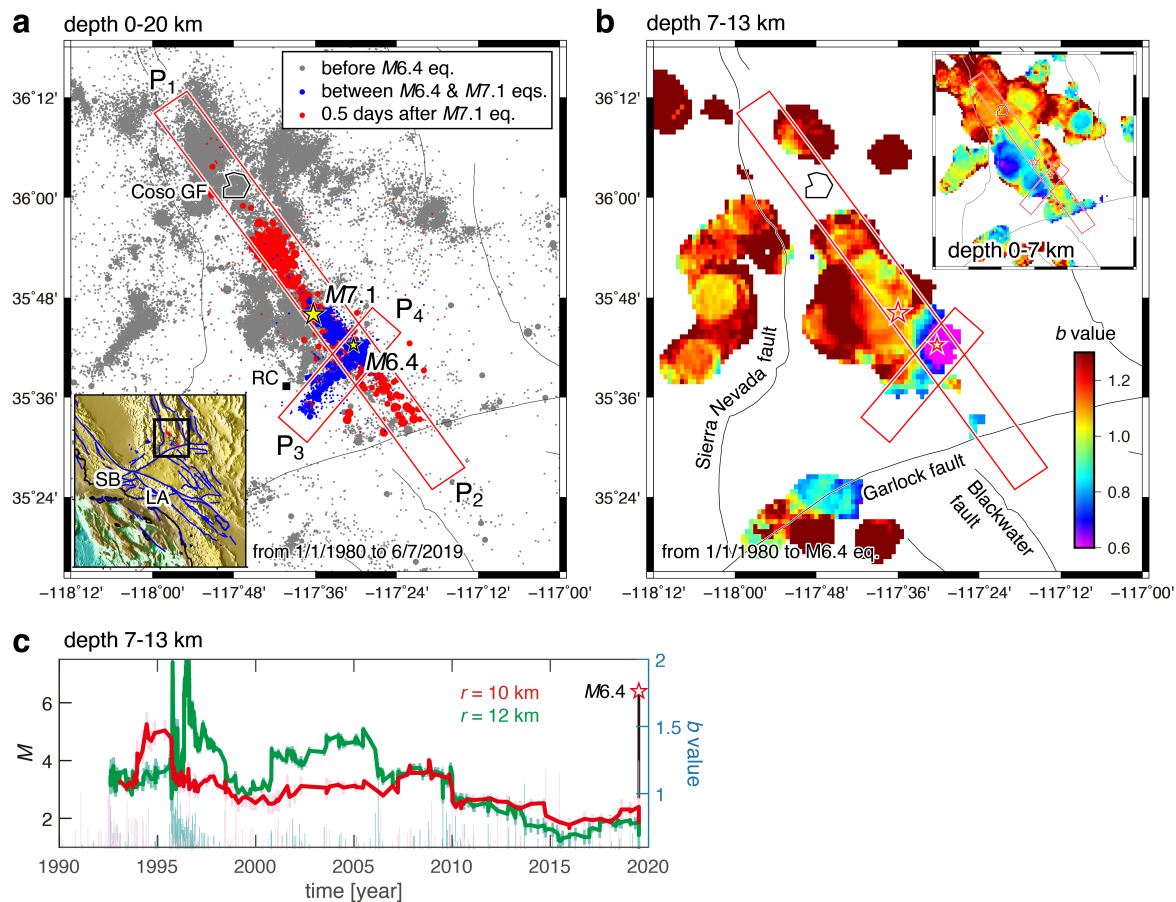


Fig. 1: (a) Map of earthquakes in the Ridgecrest region. The cross-section in Fig. 2 extends from P₁ to P₂ and from P₃ to P₄ with a width of 8 km. Inset shows the study region (black rectangle). Thin lines indicate major mapped faults. Los Angeles, Santa Barbara, Ridgecrest, and Coso geothermal field are indicated as LA, SB, RC, and Coso GF, respectively. (b) Map of b -values obtained from seismicity ($M \geq 1$) at a depth of 7-13 km before the $M6.4$ quake. Inset: the b -value map at a depth of 0-7 km. (c) Plot of b as a function of time before the $M6.4$ quake for seismicity (depth of 7-13 km) falling in the circle with a radius of $r = 10$ km (red) and 12 km (green), centered at the $M6.4$ epicenter. Moving windows cover 100 events. Also included is the magnitude-time dependence.

A map view (Fig. 1b) based on seismicity before the $M6.4$ quake with a depth range of 7-13 km shows a zone of low b -values ($b \sim 0.6$) around the future hypocenter of depth 10.7 km. Shallow seismicity (depth of 0-7 km) shows no clear zone of such low b -values near the future epicenter (inset of Fig. 1b). The low- b -value zone was seen, even when the $M4.0$ quake and its following events that occurred during the last 30 minutes before the $M6.4$ quake near the eventual hypocenter were excluded from the mapping. For earthquakes around the $M6.4$ epicenter (Fig. 1c), the b -values were mostly above 1 until 2010. Since 2010, the b -values have shown a gradual decrease over time, to values near 0.7. The final values are remarkably similar to those immediately before the entire fracture, as was obtained in a previous laboratory experiment (Lei, 2003).

CROSS-SECTIONAL VIEWS OF B-VALUES.

The $M6.4$ quake ruptured conjugate faults: the 6-km-long northwest-trending fault first slipped, followed by a slip in the ~ 15 -km-long southwest-trending fault. The initial portion of the $M6.4$ quake terminated about 4 km from the eventual $M7.1$ hypocenter. This 4-km gap was progressively filled by a series of moderate-sized earthquakes in the 34 hours after the $M6.4$ quake, which suggests that this portion of the fault acted as a barrier through which the $M6.4$ rupture was unable to propagate. This was confirmed by the cross-sectional views (Fig. 2a, b) for the pre- $M6.4$ -quake period. Low b -values ($b < 0.9$; purple to blue) were seen near the $M6.4$ hypocenter, while high b -values ($b > 1$; yellow to orange) were seen near the $M7.1$ hypocenter. This was interpreted as an indication of a weakly stressed area into which the $M6.4$ rupture was not allowed to propagate.

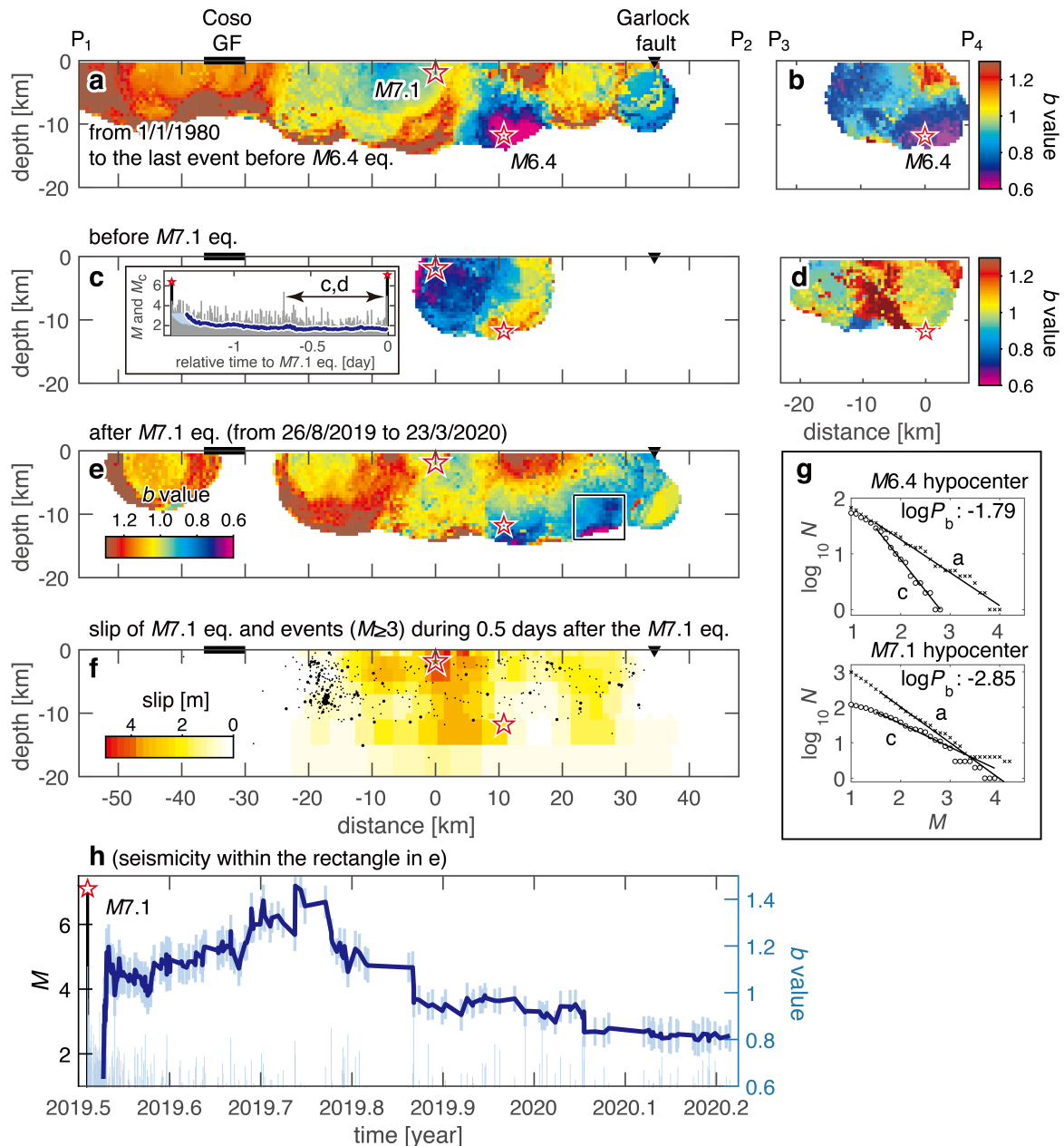


Fig. 2: (a) b -values for seismicity ($M \geq 1$) before the $M6.4$ quake along the fault ruptured by the $M7.1$ quake. Stars shows the $M7.1$ and $M6.4$ hypocenters. (b) Same as (a) for the cross-section along the fault ruptured by the $M6.4$ quake. (c, d) Same as (a) and (b) for seismicity before the $M7.1$ quake. b -values were calculated for the period indicated by c, d in the inset of (c) from the first event after the $M5.4$ quake at a relative time of -0.672 days to the last event before the $M7.1$ quake. The use of seismicity soon after the $M6.4$ quake was avoided to remove the effect of strong temporal variability in b . Inset: plot of M and completeness magnitude (M_c) as a function of time relative to the $M7.1$ quake. (e) Same as (a) for seismicity after the $M7.1$ quake. Events during the period from immediately after the $M7.1$ quake to 25 August 2019 (or

2019.65 decimal years) were not used to calculate b -values for the same reason as (c, d). (f) Slip distribution of the $M7.1$ quake, and events ($M \geq 3$) that occurred in the first 12 h. Symbol size is proportional to magnitude. (g) Top panel: frequency-magnitude distribution of earthquakes falling within a cylindrical volume with a 5-km radius, centered at the location of the $M6.4$ hypocenter in (a) and (c): a with $a = 2.44$, $b = 0.59 \pm 0.17$, and $M_c = 1.5$ and c with $a = 3.14$, $b = 1.12 \pm 0.33$, and $M_c = 1.5$. Bottom panel: same as the top one for the location of the $M7.1$ hypocenter: a with $a = 4.03$, $b = 1.01 \pm 0.07$, and $M_c = 1.6$, and c with $a = 2.86$, $b = 0.66 \pm 0.22$, and $M_c = 1.5$. Values of $\log P_b \leq -1.3$ indicate a significant difference in b . (h) Plot of b as a function of time after the $M7.1$ quake for seismicity within the rectangle in (e). Plotting procedure is the same as that for Fig. 1c.

The distribution of b -values (Fig. 2c, d) based on seismicity during a period before the $M7.1$ quake, indicated by the bidirectional arrow in the inset of Fig. 2c, shows a zone of low b -values near the eventual $M7.1$ hypocenter. A comparison with the pre- $M6.4$ -quake period in Fig. 2a, b shows that an increase in b at the $M6.4$ hypocenter and a decrease in b at the $M7.1$ hypocenter are significant (Fig. 2g). The result indicates that the $M6.4$ rupture relaxed stress near the $M6.4$ hypocenter, which had been highly stressed before the $M6.4$ quake, but that it transferred stress to the nearby region of the $M7.1$ hypocenter, which had acted as a barrier before the $M6.4$ quake. The result was the erosion of this barrier by seismicity.

COULOMB STRESS CHANGES

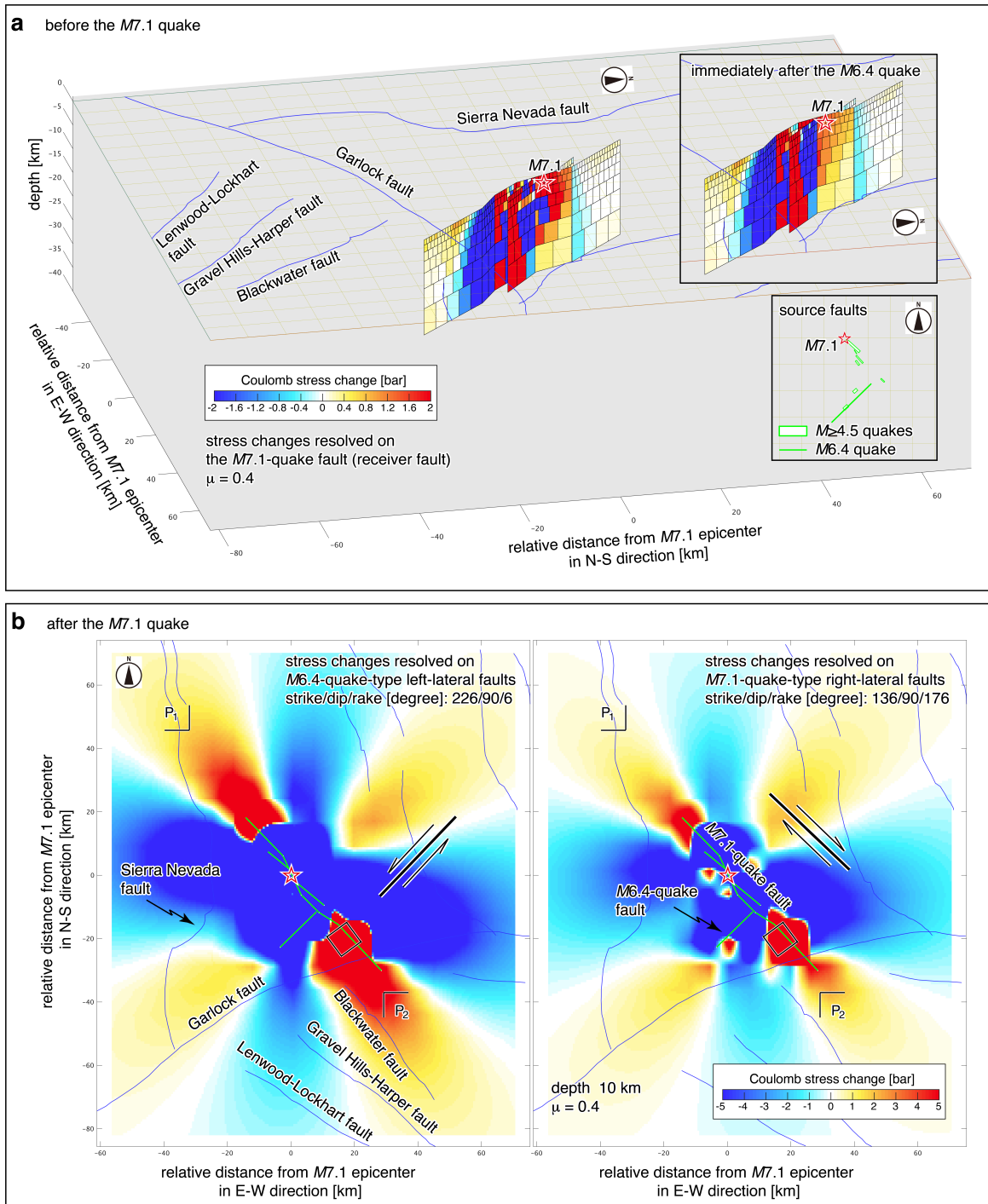


Fig. 3: (a) Stress changes resolved on the $M7.1$ quake fault as a result of the $M6.4$ quake and the following $M \geq 4.5$ events. Star indicates the $M7.1$ hypocenter. Top inset: changes in Coulomb stress as a result of only the $M6.4$ earthquake, showing that the increase in stress near the region of the $M7.1$ hypocenter was as high as 1 bar (orange). Bottom inset: source faults projected on the Earth's surface. The $M6.4$ -quake fault is indicated by a segment because it is assumed to be a vertical plane. Rectangles indicate fault planes of $M \geq 4.5$ events. (b) Changes in stress at a depth of 10 km as a result of the $M6.4$ and $M7.1$ quakes. Green segments indicate source faults ($M6.4$ and $M7.1$ quakes). Left panel: changes in stress resolved on $M6.4$ -quake-type left-lateral faults (black line with a half-arrow pair). Right panel: changes in stress resolved on $M7.1$ -quake-type right-lateral faults. The rectangle indicates an area of low b -values shown by the rectangle in Fig. 2e that displays the cross-section extending from P_1 to P_2 .

To confirm that the erosion triggered the $M7.1$ quake, Coulomb stress transfer was calculated, revealing that a region around the hypocenter of the $M7.1$ quake became about 2 bars closer to failure by the $M6.4$ quake and its subsequent seismicity (Fig. 3a). To show this map, faults of the $M6.4$ quake and the relatively large events until immediately before the $M7.1$ quake were assumed as source faults. For the $M6.4$ quake, only the southwest-trending fault was assumed. This is because a large slip of the $M6.4$ quake occurred along the southwest-trending fault rather than along the conjugate northwest-trending fault. The former fault (~15 km long) is much longer than the latter (6 km long). A comparison with a case that only considered the $M6.4$ quake as a source fault (inset of Fig. 3a) shows that the large changes in Coulomb stress near regions of the $M7.1$ hypocenter were very likely due to the $M6.4$ quake as well as its subsequent earthquakes. Even if the conjugate faults of the $M6.4$ quake were assumed as source faults, stress in the region near the $M7.1$ hypocenter increased (Stein et al., 2019).

ADDITIONAL INSIGHT INTO THE M7.1 RUPTURE NUCLEATION

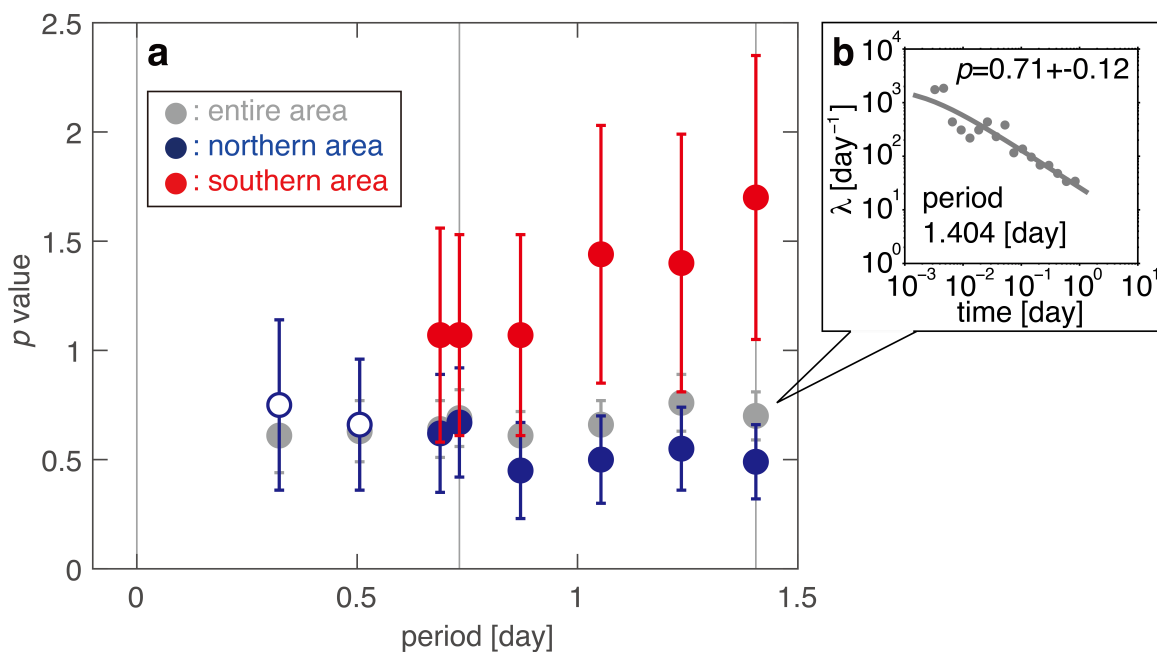


Fig. 4: Fitting of the Omori-Utsu (OU) law. (a) Plot of p -value of the OU law as a function of the length of the analyzed period since the $M6.4$ quake, based on seismicity ($M \geq 3$) during the period between $M6.4$ and $M7.1$ quakes along the fault such that the $M7.1$ ruptured in the entire area (grey), in the northern area (North of 35.72°N) (blue), and in the southern area (South of 35.72°N) (red). The maximum-likelihood fit was used to determine a p -value. Uncertainties in p were computed by bootstrapping. Open circles for the northern area show p -values obtained based on $N \leq 20$ earthquakes. For the periods ≤ 0.5 days, no p -value was obtained for the southern area, because the solution did not converge due to not enough data analyzed. Vertical lines indicating the periods of 1.404, 0.732, and 0 days correspond to the periods ending at the time of the $M7.1$, $M5.4$, and $M6.4$, quakes, respectively. **(b)** Number λ (day^{-1}) of seismicity ($M \geq 3$) as a function of time from the $M6.4$ quake for the analyzed period of 1.404 days in the entire area (grey).

Additional insight into changes in the stress state was provided by temporal behavior of the sequence following the $M6.4$ quake. Relatively large events occurred early in the post- $M6.4$ -quake sequence (grey stem plot in the inset of Fig. 2c), and the mean magnitude of these events evolved into small values over time. This behavior is well modeled by the Omori-Utsu (OU) power-law aftershock decay, given as $\lambda \sim t^{-p}$, where t is the time since the occurrence of a mainshock; λ is the number of aftershocks per unit time at t with a magnitude greater than or equal to a cutoff magnitude; and p is a constant. $p = 1$ is a good approximation, but spatio-temporal changes in p are observable. $M \geq 3$ events were used, taking homogeneity of seismicity recordings into consideration. Modeling these events showed that p was smaller for the northern area, including the $M7.1$ hypocenter, than for the southern area (Fig. 4), revealing that decay in seismicity was slower in the former area than in the latter one. This result is interpreted as an indication of a slower decrease in stress in the northern area than in the southern area, according to fictional theory (Dieterich, 1994). This supports the result of a b -value map before the $M7.1$ quake (Fig. 2c, d) that showed lower b -values (indicative of higher stress) in areas near the $M7.1$ hypocenter than in areas near the $M6.4$ hypocenter.

Low b -values near the $M7.1$ hypocenter (Fig. 2c, d), together with a temporal decay in seismicity (Fig. 4), closely match another observation of increased Coulomb stresses near the $M7.1$ hypocenter (Fig. 3a). The sequence of stress jumps caused by the $M6.4$ quake and its subsequent events resulted in an increase of roughly 2 bars. This value is not surprising and is comparable to that obtained in previous studies (Stein et al., 2019; Chen et al., 2020).

To support the observation that the events preceding the $M7.1$ quake very likely played a role in triggering the eventual $M7.1$ event, an independent analysis from the above stress-related analyses was conducted. This was achieved by investigating if any sign indicative of the $M7.1$ quake could be found in the spatial organization in seismicity after the $M6.4$ quake. According to a

previous study (Lippiello et al., 2012), the spatial concentration of smaller magnitude events (retrospectively named foreshocks) near the eventual event (retrospectively named mainshock) was a common feature of large earthquakes in southern California. To examine whether this was observed for the $M7.1$ quake, the quantity $\phi = R^{-1}/R_b^{-1}$ was selected, where R^{-1} represents the inverse distance from position x to an event that occurred before a given time, averaged over the last n events before this given time, and R_b^{-1} is the same as R^{-1} but the average is taken over the second-to-last n events. $\phi > 1$ indicates a concentration of seismicity before the given time in an area surrounding x , and $\phi < 1$ indicates the dispersion of seismicity. A cross-sectional view (Fig. 5) of ϕ -values with $n = 25$ (a typical value for southern California) at the time immediately before the $M7.1$ quake shows a region of seismic concentration ($\phi \sim 1.5$) near the hypocenter of this quake. Similar to the p -value analysis, $M \geq 3$ events were used for the ϕ -value calculation. Near the future $M7.1$ hypocenter, there was a gradual increase in ϕ to values above 1, while in other regions, ϕ -values showed low values or a decreasing trend to values of $\phi \sim 1$ or below 1. These results depend weakly on n for $n = 15$ -35, as was observed in a previous study (Lippiello et al., 2012). Our results show that the spatial organization of the pre- $M7.1$ -quake sequence in a region near the eventual hypocenter was similar to that observed for previous southern California earthquakes, but it was dissimilar in other regions. This probably reflects the erosion by active seismicity toward a region near the $M7.1$ hypocenter. Thus, the spatial clustering before the $M7.1$ quake was a foreshock-type one indicative of a future mainshock, supporting the observation based on the above stress-related analyses.

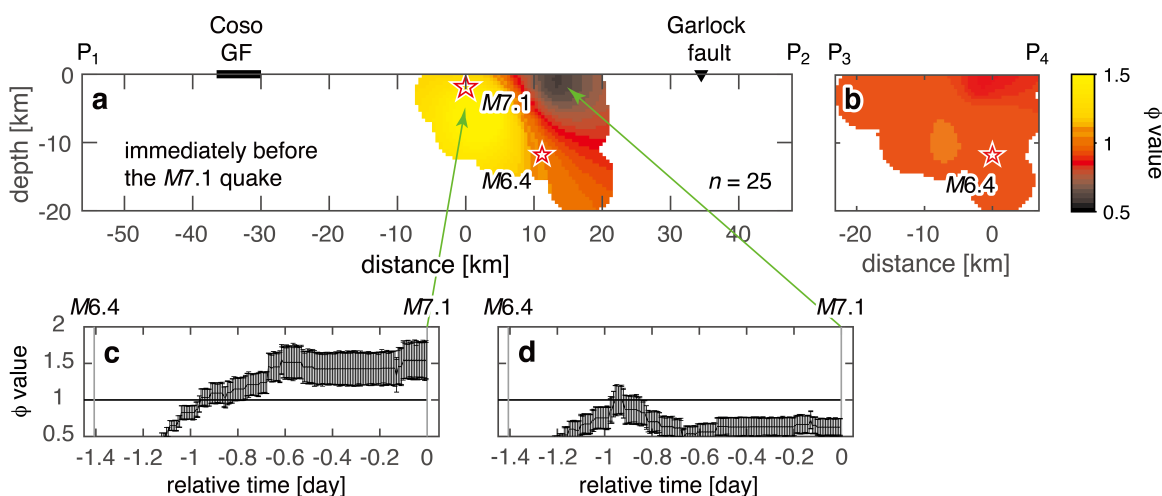


Fig. 5: Seismicity concentration/dispersion. (a) ϕ -values with $n = 25$ at the time immediately before the $M7.1$ quake, based on seismicity ($M \geq 3$) during the period between $M6.4$ and $M7.1$ quakes along the fault ruptured by the $M7.1$ quake. Note that seismicity used includes from the first event after the $M6.4$ quake to the last event before the $M7.1$ quake. Stars indicate the $M6.4$ and $M7.1$ hypocenters. (b) Same as (a) for the cross-section along the fault ruptured by the $M6.4$ quake. (c, d) Plot of ϕ as a function of relative time to the $M7.1$ quake at the locations indicated by arrows. Uncertainties in ϕ , used to draw error bars in (c) and (d), were computed by bootstrapping. The occurrence time of the $M6.4$ quake, relative to that of the $M7.1$ quake, is indicated by a grey vertical line at -1.404 days. The relative time of the $M7.1$ quake is 0 days (grey vertical line), as is obvious.

The $M7.1$ quake nucleated about 10 km to the northwest of the $M6.4$ event and its rupture propagated bilaterally, where most slips occurred near the $M7.1$ hypocenter. The pre- $M6.4$ -quake b -values (Fig. 2a) were compared with the slip distribution of the $M7.1$ quake (Fig. 2f), showing peak-slip values of 4–5 m around the $M7.1$ hypocenter (relative distance of -2 to 5 km with depth of -5 to 0 km). It was found that this peak-slip area did not overlap with high b -values ($b > 1.1$: indicative of low stress), a feature that is common to many other earthquakes. The influence of structural heterogeneity on the spatial distribution of b -values was also noted in such a way that rupture propagation of the $M7.1$ quake to the northwest terminated at an area near the Coso geothermal production field with $b > 1.1$ (red). The high-temperature area around this field may have contributed to termination of the rupture and high b -values ($b > 1.1$: red). Similar behavior was observed for the 2016 Kumamoto earthquakes (Nanjo et al., 2016).

To show that coseismic rupture, which caused stress perturbation along the fault of the $M7.1$ events, played a role in the distribution of post-seismic hazards, the slip distribution of the $M7.1$ quake (Fig. 2f) and the b -value distribution based on post- $M7.1$ -quake seismicity (Fig. 2e) were compared. An area of low b -values ($b < 0.9$: indicative of high stress), colored in blue to purple, within the rectangle shown in Fig. 2e, does not overlap with volumes of high slip (≥ 3 m: orange to red) but with volumes that remained unruptured (low slip in Fig. 2f), suggesting that the rupture of this quake released a pronounced amount of overall stress. Note that the rectangle that includes this low- b -value area is located not on the Garlock fault but near it. For events falling

within this rectangle, the b -values show a decrease over time, to values around 0.8. The values are not as low as those immediately before the $M6.4$ and $M7.1$ quakes (Fig. **1b**, **c**, and **2a-c**), but contribute the most recent values in a decreasing trend of the b -value. Similar to laboratory observations of low and decreasing b -values that could previously be detected as a fault of a few centimeters in length that approached failure (Goebel et al., 2013), this was found for natural earthquakes with faults tens of kilometers in size.

DISCUSSION: IMPLICATION OF FUTURE SEISMICITY

Given the current tectonic stress that drives the ECSZ, it is likely possible to consider that a future activated fault is the one conjugating with the $M7.1$ rupture, as seen by the $M6.4$ and $M7.1$ quake couplet. We calculated changes in Coulomb stress resolved on the $M6.4$ -quake-type left-lateral faults at a depth of 10 km (Fig. 3b), where the source faults are the right-lateral rupture of the $M7.1$ quake and the left-lateral rupture of the $M6.4$ quake. This depth of 10 km was chosen because it is a typical depth of the rectangle with the low- b -value zone in Fig. 2e. The changes in stress pull most of the nearby left-lateral-type faults further from failure (blue lobes, namely stress shadows) and push others of the same type closer to it (red lobes). We expect strong stress (red) at the region indicated by the rectangle in the left panel of Fig. 3b. Another possibility of future activation is rupture extension to the southeast: namely, the one along the fault of the $M7.1$ quake. We calculated changes in stress resolved on the $M7.1$ -quake-type right-lateral faults, revealing that faults in the zone of low b -values are again in an area with stress changes to promote failure (red lobes) in the right panel of Fig. 3b. The same stress-change calculations were conducted for different depths. The result is not induced by a bias of choice of depth: stress patterns for a depth of 8–12 km covering the rectangle shown in Fig. 2e are similar to each other.

If the zone of currently low b -values (Fig. 2e) were more stressed (decrease in b -value), seismic activity in this zone would be further enhanced with possibility of future ruptures propagating either along a $M6.4$ -quake-type left-lateral fault or along a $M7.1$ -quake-type right-lateral fault (Fig. 3b). If so, the influence of a likely future rupture on the Garlock fault would be inevitable. Although this fault has historically been seismically quiescent, it has hosted numerous large earthquakes over several thousand years, and the last major earthquake occurred about 400 to 500 years ago. Moreover, geodetic measurements showed that measurable surface creep was triggered by the Ridgecrest sequence, while no measurable creep was shown before the start of this sequence. The timing of the precursory signal observed in Fig. 2h remains unexplained: the low- b -value patch may continue or subside without the occurrence of a large earthquake. It is not yet possible to make conclusions about the quantitative predictive power of b -value mapping. Thus, together with seismological and geodetic observations, it would be worthwhile to monitor the spatio-temporal distribution of b -values around the southeast rupture terminus of the $M7.1$ quake, which contributes to seismic hazard in the ECSZ.

ABSTRACT

Monitoring stress state in the Earth's crust plays a crucial role in our understanding of an earthquake's mechanism, especially how earthquake ruptures nucleate, as well as in calculating the distribution of hazards. Crustal deformation due to the 2019 Ridgecrest earthquakes, which occurred near the town of Ridgecrest, California, that culminated in a preceding earthquake of magnitude (M) 6.4 and a subsequent $M7.1$ event, caused stress perturbation in nearby regions. However, implications of future seismic activity are still unclear. Here we analyze the occurrence of small earthquakes compared to larger ones—the b -values, showing how the nucleation area for both the $M6.4$ and $M7.1$ earthquakes had low b -values before these events occurred, and mid-to-high b -values thereafter. The slip distribution of the $M7.1$ event is also well correlated with the b -value map. Additionally, the time and local-dependent variations in b -values of the Ridgecrest earthquakes are linked with estimates of changes to Coulomb stress. The main conclusion is that the b -value mapping provide insight into the stress state in the fault zone, which is likely closely related to the nucleation and evolution of earthquakes in the sequence. The combined approach of stress-change and b -value analyses to the post- $M7.1$ -quake sequence shows an area that is currently being stressed near the Garlock fault that hosted past large earthquakes. The b -values are not as low as those immediately before the $M6.4$ and $M7.1$ events, but contribute the most recent values in a decreasing trend of the b -value. Together with geodetic and seismological observations, monitoring the spatial and temporal distribution of b -value would contribute to seismic hazards in the Eastern California Shear Zone.